Manuscript 4990 – Revision 2

Block-by-Block and Layer-by-Layer Growth Modes in *Corallium sp.* Skeletons

Jonathan Perrin[a,1], Daniel Vielzeuf[a], Angèle Ricolleau[a], Hervé Dallaporta[a], Solène Valton[b], Nicole Floquet[a]

[a] Aix-Marseille University, CNRS, CINaM UMR7325, 13288, Marseille, France

[b] RX Solutions 27 rue de Saturne – ZAC Altaïs 74650 Chavanod, France

[1] Corresponding author J. Perrin.
Address : CNRS, UMR7325, Aix-Marseille University, CINaM, 13288, Marseille, France.
E-mail addresses : perrin@cinam.univ-mrs.fr (J. Perrin), vielzeuf@cinam.univ-mrs.fr (D. Vielzeuf), ricolleau@cinam.univ-mrs.fr (A. Ricolleau), dallaporta@cinam.univ-mrs.fr (H. Dallaporta), solene.valton@rxsolutions.fr (S. Valton), floquet@cinam.univ-mrs.fr (N. Floquet).

ABSTRACT

Understanding the dynamics of biomineral growth is a challenging goal of biomineralogy that can be achieved in part by deciphering biomineral structures and chemistries. The morphology, structure and chemistry of six skeletons of Corallium and Paracorallium species (C. rubrum, C. elatius, C. johnsoni, C. niobe, P. japonicum, and P. thrinax) from the Mediterranean, the Atlantic and the Pacific oceans have been studied by X-ray micro-computed tomography, polarized light microscope, scanning electron microscope, and electron microprobe. All species have two types of biomineral structures: an inner skeleton and sclerites which are small grains of Mg-calcite found in the living tissues surrounding the skeleton. All skeletons display a central core surrounded by an annular domain. In the species studied by electron microprobe (C. rubrum, C. elatius, and P. japonicum), the central core and the annular domains display different chemical compositions with the core richer in magnesium and poorer in sulfur than the annular domain. In terms of structure, special emphasis has been put on central cores for which little data are available. The central cores are made of sclerites and sclerite aggregates within a cement consisting of fine layers of Mg-calcite. On the other hand, the annular parts are made of fine concentric layers of calcite crystallites with only rare sclerites. These contrasting features imply two different growth modes: (1) a 'block and cement' mode taking place at the apex of a branch and associated with a fast axial growth rate (~2 mm/yr); and (2) a layer-by-layer mode occurring below the apex and associated with a slow radial growth (~0.2 mm/yr). The change from a growth mode to another is anatomically controlled by the presence of a continuous network of gastrodermal canals around the sub-apical skeleton, preventing to a large extent the aggregation of sclerites. It is generally accepted that the Coralliidae family exhibits different types of skeletogeneses. In contrast with this idea, we observe that all studied Corallium species display remarkable similarities in terms of skeletogenesis and a unifying growth model for the Corallium genus is proposed. Similarities and differences with previous models are discussed. The present study shows that the morphological criterion initially used to establish the genus Paracorallium in the Coralliidae family is inadequate.

Key words: *Corallium*, *Rubrum*, *Japonicum*, *Johnsoni*, Skeletogenesis, Block and cement, Layer-by-layer, Biomineral growth

Introduction

Understanding the growth modes of biomineral structures is a major and challenging goal of biomineralogy. This task is complicated by the fact that biominerals display modular organizations at different spatial scales. The presence of hierarchical levels raises important questions: can a modular organization result from a modular construction? Is the hierarchy of structures in biominerals the result of a single or several growth mechanisms? Are these mechanisms different at nano- micro- and macro-scales? We address these questions through the example of the Mediterranean red coral (*Corallium rubrum*), and other *Corallium* (*Corallium elatius, C. johnsoni, C. niobe*) and *Paracorallium* species (*Paracorallium japonicum, P. thrinax).*

In *Corallium rubrum*, as in all *Corallium* and *Paracorallium* species, two major biomineral structures coexist: the axial skeleton and the sclerites (Fig. 1). The axial skeleton displays a complex, often planar, arrangement of branches (Fig. 1a). The internal structure of the skeleton is composed of a central cross-shaped region (Grillo et al., 1993; Lacaze-Duthiers, 1864; Marschal et al., 2004), hereafter referred to as the central core. The central core is surrounded by an annular domain composed of crenulated concentric growth rings with tortuous interfaces reminiscent of the external surface of the skeleton. Indeed, the crenulated skeleton surface is covered with uniformly distributed microprotuberances (Grillo et al., 1993; Vielzeuf et al., 2008; Weinberg, 1976). Internally, the concentric layers of the annular domain are made of submicrometer crystalline units (~80 nm). Sclerites, the second biomineral structure of *C. rubrum*, are small (up to 90 µm long) complex-shaped grains of Mg-rich calcite (~13 mol% $MgCO_3$) found in the living tissues surrounding the axial skeleton (Fig. 1c) (Grillo et al., 1993; Lacaze-Duthiers, 1864; Weinberg, 1976). Sclerites are made of thin layers of Mg-calcite crystallites of sub-micrometer size (~80 nm) (Floquet and Vielzeuf, 2011; Floquet and Vielzeuf,

2012). The presence of two distinct biomineral structures in *Corallium rubrum* (i.e. axial skeleton and sclerites) with the possibility of genetic relationships between them has attracted the interest of the scientific community for a long time. The hypothesis that the '*calcareous skeleton of C. rubrum is composed of sclerites cemented inseparably to form a continuous, unsegmented axis*' (Bayer, 1996) is classically attributed to Lacaze-Duthiers who presented a comprehensive series of observations in his monography on the 'Histoire Naturelle du Corail' published in 1864. However, Grillo et al. (1993) demonstrated that contrary to what was proposed by Lacaze-Duthiers (1864) and Weinberg (1976), microprotuberances on the skeleton surface were not sclerites embedded in the skeleton. This observation led Grillo et al. (1993) to a conclusion [previously suggested by Dantan (1928)] that sclerites are definitely incorporated at the tip of the branches, as suggested by Lacaze-Duthiers (1864), but characteristically absent from the annular part. While the structure of the annular part is now well characterized (Grillo et al., 1993; Vielzeuf et al., 2008), the internal structure of the central core which corresponds to an ancient tip of a branch, remains to be described.

Concerning other *Corallium* species, Lawniczak (1987) presented evidence that the axis of *C. johnsoni* is initially composed of fibrous calcitic crystals, then secondary lamellar overgrowths, without participation of sclerites. This observation led this author and subsequently Grillo et al. (1993) to consider the possibility that the *Coralliidae* family might exhibit different types of skeletogeneses. Bayer and Cairns (2003) reached the same conclusion and considered probable that sclerites have an insignificant or nonexistent role in axis formation of *Paracorallium* species. However, this proposal remains to be demonstrated.

Several questions arise concerning the skeletogenesis of *Corallium* species: what is the exact growth mechanism of the *C. rubrum* skeleton? Can sclerites be identified within the central core of the skeleton? Do sclerites play a large, minor or no part in the formation of the annular

part of the skeleton? And finally, is there a unifying scheme for the skeleton construction of *Corallium* and *Paracorallium* genera? These questions are addressed below.

Materials and Methods

Colonies of *C. rubrum* were collected along the rocky coast of the Mediterranean Sea between Marseille and Cassis (France). Colonies of *C. elatius* and *P. japonicum* come from various locations in Tosa Bay (Shikoku, Kochi, Japan). Other samples of *C. elatius* and some samples of *P. japonicum* of unknown origin come from a jeweller's private collection. Samples of *C. johnsoni* and *C. niobe* from the reference collection of the marine diversity of the Azores (Department of Oceanography) were collected at various locations and various depths in the archipelago of the Azores. Finally, the sample of *P. thrinax* is the paratype MNHN-Oct-243 from the collection of the Museum National d'Histoire Naturelle – Paris; the sample was collected in the vicinity of New Caledonia in the Pacific Ocean during the BIOCAL program conducted in 1985 and was first studied by Bayer (1996) and Bayer and Cairns (2003).

These samples were studied with polarized light microscope, X-ray tomography, electron microprobe (EMP) and scanning electron microscope (SEM). Organic tissues surrounding the skeleton were chemically removed by immersion in sodium hypochlorite (5%) for a few hours, and the sclerites were rinsed a few times with demineralized water then ethanol, and dried at room temperature. Skeletal apical and sub-apical parts were studied with a polarized light microscope Zeiss Axio Scope A1 (transmitted and reflected light). In some cases, the samples were cut perpendicular or parallel to the main axis of the branch without removal of dried organic tissues, and directly mounted and polished in epoxy to preserve mutual relationships between skeleton, organic tissues and sclerites.

X-ray Micro-Computed Tomography (μ-CT) is a non-destructive method for both the organic tissues and the biomineral structures. The coral samples were scanned at 9 μm resolution on a DeskTom tomograph and at 2 μm resolution on an EasyTom Nano for 4 hours (RX Solution, Annecy). Three-dimensional rendering was obtained using the Avizo software (VSG group) with its internal color map library.

Images of coral skeleton surfaces were obtained with Field Emission Scanning Electron Microscopes (FESEM) using secondary electron (SE) (JEOL 6320F and Raith Pioneer at CINaM, Marseille; LEO 1550VP at Caltech, Pasadena). Samples were carbon coated and operating conditions were 3 to 15 kV accelerating voltage and 6 to 15 mm working distance at Marseille, and 10 kV accelerating voltage, 3 mm working distance at Caltech. Images obtained with BackScattered Electrons (BSE) were made on polished sections embedded in epoxy, with 20 kV accelerating voltage, 9.5 nA probe current and 6 mm working distance. In BSE mode, the image contrast mostly depends on the sample composition: high average atomic number materials appear brighter than low Z materials and holes appear in black. Some large-scale BSE images presented in the following are mosaics of numerous small-scale images processed to homogenize contrast levels.

Electron Microprobe (EMP) chemical images of magnesium and sulfur were obtained on two different instruments: a SX100 Cameca electron microprobe (Laboratoire Magmas et Volcans, Clermont-Ferrand) and a JEOL JXA 8200 instrument (Division of Geological and Planetary Sciences, Caltech, Pasadena). The definition of X-ray images is usually 512×512 pixels with beam current, counting times, and step interval in the range 30-50 nA, 30-50 ms, 1-5 μm, respectively. In general, four to five images were acquired at the same time during sessions that lasted ~8 hours. All samples were coated with a ~20 nm thick carbon layer.

Results

Morphology, structure and texture of C. rubrum skeleton

The apex of C. rubrum skeleton

A colony of *C. rubrum* with different branches and dried tissues surrounding the skeleton is shown in Fig. 1a. The apical part of a branch with its preserved tissues has been scanned with a tomograph at a 9 µm resolution. Figure 1b is a 3D reconstruction of the skeleton surface. The contrast has been selected to enhance the morphological features of the skeleton; however, the surrounding organic tissues containing the sclerites can still be observed. Two-dimensional sections across a thin tip are shown in Fig. 2. On these slices, the relative position of the solid inner skeleton, the organic tissues with their sclerites and the polyp emplacements are observed. As noted in previous studies (Grillo et al., 1993; Lacaze-Duthiers, 1864; Vielzeuf et al., 2008) the first 3 to 10 mm upper part of the skeleton (without the organic tissues) is thinner than the sub-apical skeleton (Fig. 2a) and shows elongated depressions with crenulated margins (Fig. 2, see also Fig. 1d, Vielzeuf et al., 2008). The complex organization of the organic tissues associated with the sclerites has been described in detail by Grillo et al. (1993). For the sake of simplicity, the organic-inorganic layer containing the sclerites will be considered here as a whole and referred to as the mineralized organic layer (MOL). As noticed by previous authors, the number of polyps is higher at the apex than below it, which explains why the branch tip of an alive colony is wider than the sub-apical part (Grillo et al., 1993; Lacaze-Duthiers, 1864). The mineralized organic layer shows the presence of a dense superficial network of canals (Fig. 2b, white arrows) with complex organization (to be distinguished from the deep canal network that will be discussed later). Figure 2 also shows that the mineralized organic layer is not present underneath the polyps (i.e. at the immediate interface between the skeleton and the polyp) and thus, not in contact with the skeleton at such locations. On the contrary, between the polyps, the

mineralized organic layer is in direct contact with the skeleton (Fig 2a white circles, 2c white arrows). Concerning the tip, it should be noted that its morphology is variable (Lacaze-Duthiers, 1864): in some cases, the grooves are well-marked and look like 'calices' while in other cases, the depressions are fainter. Nevertheless, in all cases the shapes of the depressions change progressively towards the base of the branch: they become less elongated and shallower (see Fig. 1b, Vielzeuf et al., 2008). These depressions correspond to emplacements of polyps. Polarized light microscopy shows that the skeleton tip is granulated, porous and friable, and made of sclerites and larger elongated units a few hundreds of micrometers long (100 to 250 μm). These elongated units, themselves made of sclerites will be referred to as 'sclerite aggegates'. They are delicately welded together and porous space is often present between them. Sclerite aggregates are also observed along the edges of the polyp cavities (Fig. 1b, arrowed). Secondary electron SEM images in Fig. 3 show that the skeleton apex is made of sclerites with their characteristic morphologies (Fig. 3b). These sclerites are embedded within layers of Mg-calcite. Towards the sub-apical part of the skeleton and as the girth of the axis increases, less and less embedded sclerites are observed and microprotuberances appear at the surface of the skeleton (see also Fig. 6a, Vielzeuf et al., 2008).

The central core of C. rubrum skeleton

As the apex of the skeleton is made of aggregated sclerites, sclerites should be also observed in the central core of mature branches. Indeed, immunolabeling of the organic matrix of a section of *C. rubrum* indicated the presence of sclerites in the central core (Debreuil et al., 2011a). However, these images do not provide a precise idea of the inner structure of the central core. Figure 4a is a backscattered electron SEM image of the central core of a skeleton section cut perpendicular to the vertical axis. The central core displays four depressions, probable locations

of ancient polyps at early stages of the colony development. In Fig. 4a, the central core is darker than the annular part indicating an overall enrichment in lighter elements (higher Mg/Ca ratio). Indeed, the EMP chemical image shown in Fig. 4c confirms that, on average, the central core of this sample is richer in magnesium than the annular part (~13 ± 1 and ~11.5 ± 1 mol% $MgCO_3$, respectively). On the other hand, the EMP chemical image of sulfur shown in Fig. 4d indicates that the central core is globally poorer in sulfur than the annular part (~2500 ± 200 and ~2800 ± 200 ppm, respectively). The presence of numerous closed shape units inside the central core, as seen in Figs 4a and b is another major point of interest. These units display concentric chemical zoning (Fig. 4b, white arrow). Both the shape and the chemical features of these units indicate that they correspond to sclerites embedded within calcitic cement. The central core and the annular layers can also be observed on the longitudinal section of the tip of a branch (Fig. 5a). Figure 5b displays the complex boundary between the central core containing sclerites and the annular part composed of thin calcitic layers. On this image, a sclerite aggregate can be identified (dotted white line); it is characterized by a relatively homogeneous chemical composition. Sclerite aggregates can be also observed directly within the tissues with µ-CT, and with SEM after separation from the organic tissues. Such aggregate is shown in Fig. 5c; it displays numerous microprotuberances on its surface. Thus, various structures with different levels of layering are observed within the central core: sclerites display an internal structure made of calcite layers (referred to as sclerite calcitic layers) and can be themselves embedded within a calcitic cement to form a sclerite aggregate. In turn, these sclerite aggregates (and also separate sclerites) are embedded within layers of calcite (referred to as central core calcitic layers) to form the central core. The calcitic material that 'cements' the sclerites together is made of crystallites similar to those, which form sclerites. The central core calcitic layers are often discontinuous in space and cannot be followed over long distances because of their complex geometries (Fig. 5b).

The continuous white line in Fig. 5b emphasizes the boundary between the central core and the annular part. The change of layering pattern and the systematic presence of sclerites in the core are taken as indications of the boundary location between the two domains. To summarize, the core is composed of a hierarchy of internal structures composed of sclerites, sclerite aggregates, and layers of cement, with bulk chemistry slightly different from the annular part.

The annular domain of C. rubrum skeleton

The sub-apical part of a branch of *C. rubrum* displays a more regular shape than its apex (Grillo et al., 1993; Lacaze-Duthiers, 1864), and is characterized by the presence of longitudinal crenulations running along the skeleton (Grillo et al., 1993; Vielzeuf et al., 2008). Gastrodermal canals belonging to a deep canal network are located in these crenulations (Fig. 1c). This deep canal network is absent at the tip of a branch and appears progressively within the first 5 to 10 mm from the tip. In the sub-apical part of the skeleton, larger depressions not as pronounced as the ones at the tip of a branch and with a more regular shape are observed. They mark the location of the polyps (Grillo et al., 1993; Vielzeuf et al., 2008). The surface of the entire sub-apical skeleton is riddled with regularly spaced microprotuberances (ca 700/mm^2 – Grillo et al., 1993). Inside the skeleton, the growth rings of the annular domain are marked by variations of color (Lacaze-Duthiers, 1864), concentration of organic matrix (Marschal et al., 2004) and variations of magnesium and sulfur contents (Vielzeuf et al., 2008; Vielzeuf et al., 2013). An annual periodicity of the growth rings has been demonstrated for the organic matrix rings (Marschal et al., 2004) and for the magnesium and sulfur rings (Vielzeuf et al., 2008). Figure 6a is an EMP chemical image of magnesium of the skeleton and the organic tissues surrounding it. The growth rings are parallel to the surface of the skeleton and reproduce the characteristic crenulations and microprotuberances observed at the surface. Various facts concur to consider

that the annular domain is predominantly the result of the stacking of layers made of calcite crystallites, and not an agglomeration of sclerites cemented together. They include (1) the presence of calcitic thin layers (<1 μm), thinner than a sclerite (>10 μm), (2) the morphological differences between sclerites (closed morphology) and microprotuberances (open morphology), and (3) the layering continuity in and out of the microprotuberance (Fig. 6b). However, can sclerites be also present within the annular domain? Figure 6b is a backscattered electron image at the margin of a longitudinal section of skeleton. The succession of growth rings with their characteristic microprotuberances can be observed. Within these rings, two darker and closed-shape structures are observed, including one at the surface of the skeleton (right-hand side of the image). The morphology and the chemical pattern indicate that these structures are sclerites embedded within calcitic annular layers. This image demonstrates the infrequent but possible incorporation of sclerites within the annular part. The proportion of sclerites in the annular domain is difficult to evaluate; on the basis of some SEM images, we estimate it to be less than 1 vol%.

Morphology and structure of other Corallium sp.

So far, this study focused on three main aspects: the presence of sclerites in the central core of the skeleton of *C. rubrum*, the potential aggregation of sclerites into sclerite aggregates before their incorporation in the central core, and the presence of some sclerites embedded within the annular domain. Are these features observed in other *Corallium* or *Paracorallium* species? We will consider the cases of *C. elatius,* and *P. japonicum,* and to a lesser extent *C. niobe, C. johnsoni, and P. thrinax.*

Corallium elatius

Figures 7a and b are two EMP chemical images of magnesium of a perpendicular section of *C. elatius* at two different spatial resolutions. At lower resolution, a Mg-rich core is observed. At higher spatial resolution, sclerites are visible in the central core: they are richer in Mg than the embedding material (Fig. 7b); they are also poorer in sulfur as already observed in the case of *C. rubrum* (compare Fig. 7c and 4d). Figures 8a and 8b are SEM-BSE images of the central core of *C. elatius* showing sclerites embedded within central core calcitic layers. These sclerites display internal chemical oscillations emphasizing a layered structure (Fig. 8b). An enlargement of the central core layers showing characteristic layering patterns is presented in Fig. 8c. Finally, a careful examination of a section of *C. elatius* perpendicular to the axis of the skeleton shows the presence of scattered sclerites within the annular zone (Fig. 8d). Thus, similarly to *C. rubrum*, sclerites are present in large proportion within the central core, and observed occasionally within the annular part in *C. elatius*.

Paracorallium japonicum

Attempts to identify the growth rings of *P. japonicum* have been made by Hasegawa et al. (2010) (their Fig. 4) using calcium EMP mapping and also X-ray fluorescence on the Spring-8 synchrotron. On these chemical images, the presence of rings remains ambiguous and the authors conclude that Ca is almost homogeneously distributed. On the other hand, Nonaka et al. (2012b) unambiguously showed the presence of growth rings on decalcified and stained sections. This observation has been confirmed by EMPA (Hasegawa et al., 2012) and micro X-ray fluorescence (Nguyen et al., 2014). Figure 9 displays EMP chemical maps of a section of *P. japonicum* skeleton perpendicular to its axis. The core with a typical three-pointed star shape can be distinguished from the annular part. Incidentally, it should be noted that the cores of *P. japonicum* are often off-centered and that the thicknesses of growth rings around them are

298 commonly irregular. The core is on average richer in Mg and poorer in S than the annular part
299 (Figs. 9b and c). However these chemical contrasts are not as obvious as in *C. rubrum* or *C.*
300 *elatius.* The SEM images of a perpendicular section of *P. japonicum* (Fig. 10) show that the core
301 of *P. japonicum* is made of sclerites. Figure 10b is a magnification of the core; it shows sclerites
302 and their internal layered structure. On this image, core layers wrap around the sclerites and
303 develop a microprotuberance on top of a sclerite tubercle (white arrow in Fig. 10b). In the
304 annular part of *P. japonicum,* the alternation of Mg-rich and Mg-poor bands underlines the
305 growth rings (Fig. 10). The length of oscillations (ca 100 to 130 µm) is in agreement with those
306 measured by Luan et al. (2013) by organic matrix staining. The crenulations along the rings are
307 not systematically observed. In some cases, they are obvious (Fig. 9a, white arrows) while in
308 other places they seem to be absent. In all cases, these crenulations are not as marked as in *C.*
309 *rubrum*. Finally, it is important to note that some sclerites are observed here and there within the
310 annular part (Fig. 10c - inset).

311 *C. johnsoni, C. niobe, and P. thrinax*
312
313 Figures 11a, c, e show backscattered electron images at relatively low spatial resolution of
314 perpendicular sections of *C. johnsoni*, *C. niobe* and *P. thrinax*, respectively. These images
315 indicate that the three species share a common organization based on a central core with concave
316 shapes towards the outside, surrounded by an annular domain. Images at higher resolution (Figs.
317 11b, d, f) point out the presence of numerous sclerites within the core. *C. johnsoni* and *C. niobe*
318 have a central core composed of a relatively large proportion of sclerites while *P. thrinax* seems
319 to display fewer sclerites per surface unit. The interface between central cores and annular
320 regions is not always obvious: in some cases the transition is abrupt and clearly visible while in

other cases a progressive transition is observed. Nevertheless, the change of layering pattern and the appearance of microprotuberances are still good indicators of the transition.

As in previous cases, isolated sclerites have been observed in the annular part of *P. thrinax*. In two other *Corallium* species (*P. inutile* and *C. kishinouyei*), formerly published SEM images can be re-interpretated as sclerites or sclerite aggregates being occasionally incorporated at the surface of the sub-apical skeleton (Fig. 40 in Nonaka et al., 2012a). To conclude, all studied *Corallium* species display distinct central cores and annular domains, with abundant sclerites in the central core, and rare but systematically present sclerites in the annular part.

Discussion

The skelogenesis of C. rubrum

A dynamic model of axial growth

The tip of a *C. rubrum* branch is the location of intense biological and mineralization activities, as indicated by the presence of a bulbous shape associated with a larger number of polyps and sclerites than along the sub-apical portions of the branch. Previous studies showed that octocoral sclerites form within cells or clusters of cells (i.e. scleroblasts); once formed, it is generally assumed that sclerites are expelled from the scleroblast and grow extracellularly [see Kingsley and Watabe (1982) for *Leptogorgia virgulata* and Goldberg and Benayahu (1987) for *Pseudoplexaura flagellosa*]. Our data show that in the case of *C. rubrum*, some sclerites coalesce and are coated with fine layers of calcite to form larger units: the sclerite aggregates (Fig. 5c). At the tip of a branch, the mineralized organic layer containing the sclerites is locally in direct contact with the consolidated skeleton (see Fig. 2a, white circles). At this stage, an important question is to determine whether sclerites either move toward the tip of a branch to expand it or, conversely, act as more or less immobile nuclei in the mineralized organic layer and are

345 progressively trapped and cemented together to extend the tip (forefront nucleation and growth).
346 The mechanism of forefront nucleation and growth is in better agreement with the absence of
347 gradient of sclerite concentration in the MOL toward the tip and the fact that non-rigid elongated
348 twigs of *C. rubrum* up to 10 cm long have been reported (P. Raffin, Pers. Comm. 2012 and
349 Lacaze-Duthiers 1864, p. 66). This last observation points out a temporary absence of
350 consolidated axial skeleton, a situation that is permanent in some octocorals (Bayer, 1956).
351 Figure 12a is a schematic model of skeleton growth at the tip of a branch in a longitudinal
352 section. Three related sections perpendicular to the main axis of the skeleton at different stages of
353 growth are also shown (Figs. 12b-d). The first step of apex expansion corresponds to the
354 confinement between the polyps of the mineralized organic layer containing the sclerites. Within
355 the mineralized organic layer, sclerites can aggregate into larger units (sclerite aggregates) or not.
356 Then, as mineralization proceeds, sclerite aggregates or isolated sclerites are coated, then
357 cemented together to finally coalesce with the tip of the consolidated branch. During the early
358 stage of sclerite aggregate formation, it should be noted that the growth is multi-directional.
359 Then, the cementing of sclerite aggregates and separate sclerites generates a progressively more
360 continuous, less porous and less fragile tip. Interestingly, the overall unidirectional growth of a
361 branch tip is in part the result of local multidirectional growth of block units progressively
362 cementing together. This process could explain the complex layering pattern of the central core.
363 As growth proceeds, the deposited layers become less chaotic, more continuous and involve less
364 and less sclerites. Concomitantly, regularly spaced microprotuberances appear at the surface of
365 the layers indicating a change of growth regime. The trivial image of 'block and cement' can be
366 used to describe the central core structure of *C. rubrum*. In our mind, both separate sclerites and
367 sclerite aggregates are 'blocks'. The blocks and the cement are made of the same calcitic
368 material, the formation of blocks predates their cementing, and the sclerites have interlocking

morphologies adding to the mechanical resistance of the material. Interestingly, the concept of 'block and cement' accounts for both the structure and the construction mode of the central core of *C. rubrum*.

A model for the radial growth

As noted earlier, the annular domain of *C. rubrum* is characterized by the presence of concentric growth rings parallel to the skeleton growth surface. Variations of calcium, magnesium, sulfur, strontium and organic matrix point out the addition of rings of variable compositions with time (Marschal et al., 2004; Vielzeuf et al., 2013; Weinbauer, 2000). The tortuous interfaces between the rings result from the presence of microprotuberances at the surface of the red coral skeleton and can be seen as paleosurfaces of growth. At large scale, the relatively homogeneous chemical layers can be recognized over long distances and allow the counting of annual growth rings (Vielzeuf et al., 2013). However, chemical images at higher spatial resolution show that the fine layers constituting the rings are not necessarily continuous over long distances (e.g. Fig. 6a, white arrows). Thus, new crystalline material is not necessarily added simultaneously over the entire surface of the skeleton. Such discontinuities along the growth front have been observed in scleractinian corals by ^{86}Sr labeling experiments (Houlbrèque et al., 2009).

From these observations, it can be concluded that the addition of more or less continuous layers of crystallites of Mg-calcite of slightly variable compositions (12 ± 2 mol% $MgCO_3$ - Vielzeuf et al., 2013) is the predominant mechanism of annular growth in the sub-apical part of the skeleton. However, sclerites play also a minor role in the radial growth. The presence of a small proportion of sclerites in the annular part may seem of little interest. However, as a working hypothesis, we can consider that sclerites incorporated at the surface of the sub-apical skeleton represent potential nuclei for secondary branches. The initiation of new secondary

branches, well below the tip of the colony, has been observed during the monitored growth of *C. rubrum* (J. Garrabou, Pers. Comm.).

Anatomic control of the change from a growth mode to another

The results presented here suggest that two rather distinct mechanisms of growth take place in *C. rubrum*: the axial growth (central core extension) is dominated by the addition of sclerites or sclerite aggregates cemented together by central core calcitic layers (block-by-block growth) while the radial growth is dominated by the addition of annular layers of calcite (layer-by-layer growth) with rare embedded sclerites. It should be stated that the two different growth modes are associated with contrasting rates observed in axial and radial growths (Debreuil et al., 2011b; Marschal et al., 2004). The diametral growth rate in the red coral has been estimated in the range 200 to 350 µm per year (Gallmetzer et al., 2010; Garrabou and Harmelin, 2002; Marschal et al., 2004; Vielzeuf et al., 2013) while the axial growth rate is about one order of magnitude higher and has been estimated around 1.8 ± 0.7 mm per year (Garrabou and Harmelin, 2002). The duality of growth mode raises the question of the change from a mechanism to another. Lacaze-Duthiers (1864) noted the existence of two distinct, though inter-connected, networks of gastrodermal canals in the living tissues of *C. rubrum*: a superficial network made of relatively small interconnected canals, and a deep network with larger canals (~200 µm) nested in the crenulations of the skeleton (Fig. 1c). The superficial network is present everywhere in the tissues (Fig. 12) but is the only network present at the tip of a branch (or during the early stages of development of the colony). In other words, the deep network is present only around the sub-apical part of the skeleton where the crenulations are observed (Fig. 12d). From these observations, it is tempting to imagine that the deep network acts as a barrier between the mineralized organic layer and the skeleton, preventing the aggregation of sclerites on the

skeleton. Thus, the change from a growth mechanism to another would be controlled by the anatomy of the organism and particularly the presence of a deep canal network. Interestingly, these canals are located within the trough of the crenulations. Between two canals (i.e. along the crests of the crenulations), the consolidated skeleton and the mineralized organic layer are closer to each other (Fig. 12d). This is where rare and isolated sclerites could be preferentially incorporated in the radial skeleton. Thus, in this scheme the deep network would be important in shaping the growth mode: when present, a layer-by-layer mode would prevail while a block-by-block process would take place otherwise. Following the same line of reasoning, it has been shown earlier that the morphology of the tip (and the central core) is connected with the spatial distribution of the polyps, and thus anatomically controlled. In consequence, radially distributed polyps at a branch tip could favor a uni-directional vertical growth, while a polyp located at the very tip of the branch could favor the emergence of a ramification (e.g. Fig. 2a). Here also, the morphology of the colony would be controlled by the anatomy of the organism. Further work is required to verify this working hypothesis.

Even if the growth mechanisms of central core and annular domain differ at macroscale, it should be stated that all the observed structures (sclerites, sclerite aggregates, central core layers, annular layers) are made of similar crystallites of Mg-calcite, and thus, that at micrometer or sub-micrometer scale the biomineralization processes are remarkably identical: the organism makes layers of calcite crystallites. Grillo et al. (1993) showed that the cellular structure secreting a sclerite (scleroblast) was identical to the epithelium surrounding the axial skeleton with respect to cellular organization and structure, and that the growth patterns and mineralogy of the axial skeleton and the sclerites were fundamentally identical. Implementing this idea, the formation of sclerite aggregates might be added as an intermediate stage. In that scheme, scleroblasts, epithelium around the sclerite aggregates, and epithelium surrounding the sub-axial skeleton

(axial epithelium) would secrete layers of calcite on sclerites, sclerite aggregates, apical or sub-apical skeletons, respectively. In all these cases, the process would be almost identical and only slight differences would appear (e.g. variations of chemical composition, layering frequency, more or less chaotic layer arrangements and slight differences in crystallographic organization).

Comparison to previous models

It has been noted in the introduction that the Lacaze-Duthiers's hypothesis for the formation of the *C. rubrum* entire skeleton is classically considered as a mere aggregation and cementing of sclerites (Allemand and Bénazet-Tambutté, 1996; Bayer and Cairns, 2003; Cuif et al., 2011; Debreuil et al., 2012; Weinberg, 1976). As a matter of fact, Lacaze-Duthiers's opinion is more subtle and deserves further examination. In order to characterize the skeletal organization of *C. rubrum*, Lacaze-Duthiers (1864) first studied early development stages of a *C. rubrum* colony ('planula' with a single polyp) and observed that the complex-shaped proto-skeleton was made of an aggregation of *'nodules of rocky substance'* and that the nodules themselves were made of aggregated sclerites (p. 183-184). Then, Lacaze-Duthiers studied the tip of a mature colony, considering that features observed in the proto-skeleton should be found at the tip of an adult branch (p. 186, 187). There, Lacaze-Duthiers observed *'perfectly regular entire sclerites, welded together on one of their sides'* (p.188). For Lacaze-Duthiers, the complex-shaped tip becomes the core of the mature axial skeleton (p. 188), which explains the complex shape of the central core. Concerning the sub-apical part of the skeleton, this author always separates a core from an annular part (p. 122). Most importantly, he points out differences between the growth of the apex and the sub-apical part, and states that the annular region around the central core forms by *'deposition of concentric layers regularly molded on top of each other'* (p. 112) which points out a centrifugal growth. Concerning the involvement of sclerites in the formation of the annular part,

Lacaze-Duthiers observed colored radial bands orthogonal to the colored growth rings in sections perpendicular to the skeleton axis (Lacaze-Duthiers, 1864, Plate VIII, and also p. 189). He attributed the color of these radial bands to local incorporation of sclerites, preferentially along ridges of the crenulations (p. 189). Thus, for Lacaze-Duthiers, sclerites play a role in the formation of the annular part (though not as important as in the central core). The presence of sclerites in the annular part has been challenged by Allemand and Bénazet-Tambutté (1996); Allemand and Grillo (1992); Debreuil et al. (2012); Debreuil et al. (2011a); Debreuil et al. (2011b); Grillo et al. (1993) who concluded that the growth of annular part of the skeleton does not involve sclerites. This conclusion was reached in part on the basis of biocalcification kinetic experiments indicating that there was no delay in the calcification of sclerites and annular skeleton as would be expected if the skeleton was made by a process of sclerite aggregation (Allemand and Grillo, 1992). A similar conclusion was reached by Vielzeuf et al. (2008) who did not observe sclerites in the annular part of the skeleton in their SEM investigations. The hypothesis of Lacaze-Duthiers was also challenged on the basis that there was no evidence of 'cement' (Grillo et al., 1993; Vielzeuf et al., 2008). On the basis of the new data presented here, the statement that sclerites are characteristically absent from the annular part and that there is no 'cement' between the sclerites must be reconsidered. Concerning the so-called 'cement', it should be stated that this concept is not presently used in the sense of a material of a different nature but in the structural sense of a material able to hold together previously built units. Lacaze-Duthiers used this term in this sense and insisted on the fact that both sclerites and 'cement' were made of the same '*limestone*' (p.122). Subsequent studies showed that the material constituting the sclerites, the sclerite aggregates and the annular layers in the skeleton were made of Mg-calcite crystallites (plus organic matrix) in crystallographic register (Floquet and Vielzeuf, 2011; Grillo et al., 1993; Vielzeuf et al., 2008). It is the macroscopic properties of the layers (morphologies,

489 width, and frequency of the layering) and not the nature of the crystallites that differ from a
490 structure to another.

491 To summarize, the model of skeletogenesis of *C. rubrum* presented here, based on new
492 structural characterization of the central core, is in-between models previously proposed by
493 Lacaze-Duthiers (1864) and Allemand and Grillo (1992). In agreement with both previous
494 interpretations, the skeletogenesis at the branch tip is dominated by the aggregation of sclerites
495 allowing a fast axial growth. Concerning the annular domain (radial growth), we demonstrate that
496 sclerites occasionally take part in the growth process. These isolated sclerites in the annular part
497 are not as abundant as suggested by Lacaze-Duthiers (1864) and our observations do not fully
498 support a preferential arrangement of sclerites along crenulation ridges, so far. Furthermore, as
499 correctly pointed out by Grillo et al. (1993), Lacaze-Duthiers erroneously interpreted
500 microprotuberances at the surface of the axial skeleton as sclerites embedded in a calcareous
501 cement (Lacaze-Duthiers, p. 189, and his Figs 38 and 38bis). As far as the incorporation of
502 sclerites in the annular part is concerned, it seems that Lacaze-Duthiers reached an almost
503 qualitatively (though not quantitatively) correct conclusion on the basis of incorrect observations.
504 On other grounds, our model puts emphasis on the aggregation of sclerites into sclerite
505 aggregates prior to the construction of branch tips, an aspect overlooked in models posterior to
506 Lacaze-Duthiers's work. The present study considers also the dynamics of sclerite aggregation
507 through a forefront nucleation and growth process at the stalk tip. Finally, our model attempts to
508 connect the skeleton morphology and modes of growths to the anatomy of the organism.

509 ***Application to other Corallium sp.***
510
511 The new data presented here on *C. johnsoni* point out an overall skeletal structure similar to *C.*
512 *rubrum*, in contradiction with previous studies (Cuif et al., 1985; Lawniczak, 1987). Furthermore,

observations on all studied *Corallium* and *Paracorallium* species (*C. rubrum*, *C. elatius, C. johnsoni, C. niobe,* and *P. japonicum and P. thrinax),* combined with previous observations, indicate the presence of sclerites (or sclerite aggregates) cemented together at the tips and the central cores of the different skeletons. Thus, the hypothesis proposed by Bayer and Cairns (2003) that sclerites have an insignificant or even nonexistent role in axis formation of *Paracorallium* species is not verified. As growth of colonies proceeds, complex-shaped central cores are overlaid with layers of Mg-calcite (plus some sclerites here and there) forming the annular parts of the skeletons. From the similarities of structure between *Corallium* and *Paracorallium* skeletons, we propose that contrary to the generally accepted idea, the skeletogenesis of the species belonging to these two genera are similar. At this stage of our knowledge, we consider that the general features of the model presented above for the skeletogenesis of *C. rubrum* apply to other *Corallium* species. As a word of caution, subtle differences in skeletogenesis from one species to another probably exist but remain to be characterized.

Implications

Although the distinction between genera and species is not normally based on morphology or growth mechanism, this structural study of *Corallium* skeletons has taxonomic implications. Indeed, in 2003, Bayer and Cairns proposed to subdivide in two genera the *Coralliidae* family on the basis of a morphological criterion: a *Paracorallium* genus (seven species including *P. japonicum, P. thrinax, PC inutile*) with *"longitudinally grooved axes and autozooids seated in distinctive axial pits with beaded margins"*, and a *Corallium* genus (nineteen species including *C. rubrum, C. elatius, C. johnsoni, C. niobe, C. kishinouyei*) devoid of these features. Furthermore, as already stated in the introduction, these authors considered that sclerites probably have a non-

existent role in axis formation of *Paracorallium* species. However, the morphological pattern used to characterize the *Paracorallium* genus is commonly observed in *C. rubrum* colonies (e.g. Vielzeuf et al. 2008, their Fig. 1d; Nonaka, 2012). This similarity of morphology sheds some doubt on the criterion used by Bayer and Cairns (2003) to subdivide the *Coralliidae* family. Moreover on the basis of molecular sequencing and phylogenetic analyses, Ardila et al. (2012) concluded that there was no support for the taxonomic status of the two currently recognized genera in the *Coralliidae* family. In order to clarify the systematic positions of *Corallium* and *Paracorallium* species, Uda et al. (2013) determined the complete mitochondrial genome sequence of *C. elatius* and *C. rubrum.* The comparison with previous results on *P. japonicum* and *C. konojoi* (Uda et al., 2011) supports the validity of a classification separating the *Coralliidae* family into the two genera, but not as proposed by Bayer and Cairns (2003). Considering the gene order arrangement and the nucleotide sequence identity, Uda et al. (2013) found that *Corallium rubrum* is closer to *Paracorallium japonicum* than *Corallium elatius and Corallium konojoi* and concluded that the currently accepted generic classification of *Coralliidae* must be reconsidered (Uda et al., 2013).

The multilevel modular mesocrystalline organization of *C. rubrum* has been discussed in a previous article (Vielzeuf et al., 2010). There, we concluded that a biomineral modular organization does not necessarily imply a modular construction. This conclusion still holds in particular for hierarchical crystallographic structures. However, it does not preclude cases of modular structures resulting from modular construction. The block-by-block construction of the central core of *Corallium* species is an example among others (e.g. coccoliths) of modular construction at meso-scale implying both intra- and extra-cellular processes. Thus, understanding the formation of *Corallium* skeletons requires the integration of various spatial scales from the understanding of the formation of calcite crystallites at the atomic or molecular scales (through

561 ACC or not) to the aggregation of tens of μm large pre-formed blocks. The combination of a
562 vertically fast-growing central core surrounded by radially slow-growing annular layers is a
563 characteristic of *Corallium* skeletons. To what extent this belted central core pattern participates
564 to the strength of the skeleton remains to be determined.
565

566

567 **Acknowledgements**

568

569 *This work has been supported by the Centre National de la Recherche Scientifique (CNRS), by*
570 *the Institut National des Sciences de l'Univers (INSU) through grant INTERRVIE 2009 to DV*
571 *and INTERRVIE 2013 to AR, by the Agence Nationale pour la Recherche (ANR) through ANR*
572 *CoRo 2011-2015, by the Centre Interdisciplinaire de Nanoscience de Marseille (CINaM) through*
573 *internal grants, and by the European Union COST action TD0903. This study benefited from the*
574 *generosity of numerous contributors who supplied rare samples. We thank P. Raffin, J.*
575 *Garrabou, and C. Marschal for C. rubrum colonies from various places in the Mediterranean. C.*
576 *Balme-Heuzes provided a wide range of precious corals from the Pacific Ocean. Samples of P.*
577 *japonicum and C. elatius were kindly provided by G. Tanaka from the Precious Coral Protection*
578 *and Development Association; we thank K. Saiki from Osaka University for initiating the fruitful*
579 *exchange with G. Tanaka. Rare specimens of C. johnsoni and C. niobe were provided by F. J. de*
580 *Mora Porteiro from the Department of Oceanography and Fisheries, University of the Azores.*
581 *Finally, we are grateful to P. Lozouet, C. Dupoux, P. Joannot, and A. Andouche from the*
582 *Museum National d'Histoire Naturelle, Paris (MNHN) for providing the paratype of P. thrinax*
583 *(MNHN-Oct-243). Many observations were made on a FESEM financed by the European Fund*
584 *for Regional Development (EFRD). We thank F. Bedu for his assistance on this instrument. We*
585 *thank Ma Chi (Caltech, Pasadena) and J. L. Devidal (LMV, Clermont-Fd) for their assistance*
586 *with electron microprobe imaging. Comments by 3 anonymous reviewers as well as efficient*
587 *editorial handling by A. Fernandez-Martinez are gratefully acknowledged. This is contribution*
588 *ANR CoRo n° 04.*

589
590

References

Allemand, D., and Bénazet-Tambutté, S. (1996) Dynamics of calcification in the Mediterranean red coral, Corallium rubrum (Linnaeus) (Cnidaria, Octocorallia). Journal of Experimental Zoology, 276(4), 270-278.

Allemand, D., and Grillo, M.C. (1992) Biocalcification mechanism in gorgonians: ^{45}Ca uptake and deposition by the Mediterranean red coral Corallium rubrum. Journal of Experimental Zoology, 262(3), 237-246.

Ardila, N., Giribet, G., and Sanchez, J. (2012) A time-calibrated molecular phylogeny of the precious corals: reconciling discrepancies in the taxonomic classification and insights into their evolutionary history. BMC Evolutionary Biology, 12(1), 246.

Bayer, F.M. (1956) Octocorallia. In R.C. Moore, Ed., Treatise on Invertebrate Paleontology, Part F, Coelenterata, p. F166-F231. Geological Society of America and University of Kansas Press, Lawrence.

Bayer, F.M. (1996) Three new species of precious coral (Anthozoa: Gorgonacea, genus Corallium) from Pacific waters. Proceedings of the Biological Society of Washington, 109(2), 205 - 228.

Bayer, F.M., and Cairns, S.D. (2003) A new genus of the scleraxonian family Coralliidae (Octocorallia: Gorgonacea). Proceedings of the Biological Society of Washington, 116(1), 222 - 228.

Cuif, J.P., Dauphin, Y., and Sorauf, J.E. (2011) Biominerals and Fossils through Time. 490 p. Cambridge University Press, Cambridge.

Cuif, J.P., Lafuste, J., and Lawniczak, A. (1985) Evolution microstructurale au cours de l'ontogenèse chez un Alcyonaire actuel: passage fibres/lamelles dans le squelette axial de Corallium johnsoni Gray (Cnidaria, Octocoralla). Comptes Rendus de l'Académie des Sciences Paris Série II, 300(5), 181-184.

Dantan, J. (1928) Recherches sur la croissance du corail rouge Corallium rubrum lamarck. Bulletin de la Societé Zoologique de France, 53, 42-46.

Debreuil, J., Tambutté, É., Zoccola, D., Deleury, E., Guigonis, J.M., Samson, M., Allemand, D., and Tambutté, S. (2012) Molecular Cloning and Characterization of First Organic Matrix Protein from Sclerites of Red Coral, Corallium rubrum. Journal of Biological Chemistry, 287(23), 19367-19376.

Debreuil, J., Tambutté, S., Zoccola, D., Segonds, N., Techer, N., Allemand, D., and Tambutté, É. (2011a) Comparative analysis of the soluble organic matrix of axial skeleton and sclerites of Corallium rubrum: Insights for biomineralization. Comparative Biochemistry and Physiology Part B: Biochemistry and Molecular Biology, 159(1), 40-48.

Debreuil, J., Tambutté, S., Zoccola, D., Segonds, N., Techer, N., Marschal, C., Allemand, D., Kosuge, S., and Tambutté, É. (2011b) Specific organic matrix characteristics in skeletons of Corallium species. Marine Biology, 158(12), 2765-2774.

Floquet, N., and Vielzeuf, D. (2011) Mesoscale twinning and crystallographic registers in biominerals. American Mineralogist, 96(8-9), 1228-1237.

Floquet, N., and Vielzeuf, D. (2012) Ordered Misorientations and Preferential Directions of Growth in Mesocrystalline Red Coral Sclerites. Crystal Growth & Design, 12(10), 4805-4820.

Gallmetzer, I., Haselmair, A., and Velimirov, B. (2010) Slow growth and early sexual maturity: Bane and boon for the red coral Corallium rubrum. Estuarine, Coastal and Shelf Science, 90(1), 1-10.

Garrabou, J., and Harmelin, J.G. (2002) A 20-year study on life-history traits of a harvested long-lived temperate coral in the NW Mediterranean: insights into conservation and management needs. Journal of Animal Ecology, 71(6), 966-978.

Goldberg, W.M., and Benayahu, Y. (1987) Spicule formation in the Gorgonian coral Pseudoplexaura-Flagellosa. 1: Demonstration of the intracellular and extracellular growth and the effect of ruthenium red during decalcification. Bulletin of Marine Science, 40(2), 287-303.

Grillo, M.C., Goldberg, W.M., and Allemand, D. (1993) Skeleton and sclerite formation in the precious red coral, Corallium rubrum. Marine Biology, 117(1), 119-128.

Hasegawa, H., Iwasaki, N., Suzuki, A., Maki, T., and Hayakawa, S. (2010) Distributions of Trace Elements in Biogenic Carbonate Minerals of Precious Corals by X-ray Fluorescence Analysis. Bunseki Kagaku, 59(6), 521-530.

Hasegawa, H., Rahman, M.A., Luan, N.T., Maki, T., and Iwasaki, N. (2012) Trace elements in Corallium spp. as indicators for origin and habitat. Journal of Experimental Marine Biology and Ecology, 414, 1-5.

Houlbrèque, F., Meibom, A., Cuif, J.-P., Stolarski, J., Marrocchi, Y., Ferrier-Pagès, C., Domart-Coulon, I., and Dunbar, R.B. (2009) Strontium-86 labeling experiments show spatially heterogeneous skeletal formation in the scleractinian coral Porites porites. Geophysical Research Letters, 36(4), L04604.

Kingsley, R., and Watabe, N. (1982) Ultrastructural investigation of spicule formation in the gorgonian Leptogorgia virgulata (Lamarck) (Coelenterata: Gorgonacea). Cell and Tissue Research, 223(2), 325-334.

Lacaze-Duthiers, H. (1864) Histoire naturelle du corail J. B. Bailière et Fils, Paris.

Lawniczak, A. (1987) Les modalités de croissance de l'axe calcaire chez Corallium johnsoni. Senckenb. Marit.(19), 149-161.

Luan, N.T., Rahman, M.A., Maki, T., Iwasaki, N., and Hasegawa, H. (2013) Growth characteristics and growth rate estimation of Japanese precious corals. Journal of Experimental Marine Biology and Ecology, 441(0), 117-125.

Marschal, C., Garrabou, J., Harmelin, J.G., and Pichon, M. (2004) A new method for measuring growth and age in the precious red coral Corallium rubrum (L.). Coral Reefs, 23(3), 423-432.

Nguyen, L.T., Rahman, M.A., Maki, T., Tamenori, Y., Yoshimura, T., Suzuki, A., Iwasaki, N., and Hasegawa, H. (2014) Distribution of trace element in Japanese red coral Paracorallium japonicum by μ-XRF and sulfur speciation by XANES: Linkage between trace element distribution and growth ring formation. Geochimica et Cosmochimica Acta, 127, 1-9.

Nonaka, M. (2012) Systematic Studies of the Indo-Pacific Corallidae. IPCF 2012 Proceeding of International Precious Coral Forum 2012, p. 70-85, Kochi, Japan.

Nonaka, M., Muzik, K., and Iwasaki, N. (2012a) Descriptions of two new species and designation of three neotypes of Japanese Coralliidae from recently discovered specimens that were collected by Kishinouye, and the introduction of a statistical approach to sclerite abundance and size. Zootaxa(3428), 1-67.

Nonaka, M., Nakamura, M., Tsukahara, M., and Reimer, J.D. (2012b) Histological Examination of Precious Corals from the Ryukyu Archipelago. Journal of Marine Biology, 2012, 14.

Uda, K., Komeda, Y., Fujita, T., Iwasaki, N., Bavestrello, G., Giovine, M., Cattaneo-Vietti, R., and Suzuki, T. (2013) Complete mitochondrial genomes of the Japanese pink coral (Corallium elatius) and the Mediterranean red coral (Corallium rubrum): a reevaluation of

the phylogeny of the family Coralliidae based on molecular data. Comparative Biochemistry and Physiology Part D: Genomics and Proteomics, 8(3), 209-219.

Uda, K., Komeda, Y., Koyama, H., Koga, K., Fujita, T., Iwasaki, N., and Suzuki, T. (2011) Complete mitochondrial genomes of two Japanese precious corals, Paracorallium japonicum and Corallium konojoi (Cnidaria, Octocorallia, Coralliidae): notable differences in gene arrangement. Gene, 476, 27 - 37.

Vielzeuf, D., Floquet, N., Chatain, D., Bonneté, F., Ferry, D., Garrabou, J., and Stolper, E.M. (2010) Multilevel modular mesocrystalline organization in red coral. American Mineralogist, 95(2-3), 242-248.

Vielzeuf, D., Garrabou, J., Baronnet, A., Grauby, O., and Marschal, C. (2008) Nano to macroscale biomineral architecture of red coral (Corallium rubrum). American Mineralogist, 93(11-12), 1799-1815.

Vielzeuf, D., Garrabou, J., Gagnon, A., Ricolleau, A., Adkins, J., Günther, D., Hametner, K., Devidal, J.-L., Reusser, E., Perrin, J., and Floquet, N. (2013) Distribution of sulphur and magnesium in the red coral. Chemical Geology, 355(0), 13-27.

Weinbauer, M.G. (2000) On the potential use of magnesium and strontium concentrations as ecological indicators in the calcite skeleton of the red coral (Corallium rubrum). Marine Biology, 137, 801-809.

Weinberg, S. (1976) Revision of the common octocorallia of the Mediterranean circalittoral. I. Gorgonacea. Beaufortia, 24, 63-104.

Figure captions:

Figure 1: Morphology and anatomy of a C. rubrum colony. (a) Colony of C. rubrum covered with its dried tissues. (b) Three-dimensional rendering of a X-ray Micro-Computed Tomography (µ-CT) reconstruction at 2 µm resolution of a C. rubrum branch tip. Elongated units made of sclerites (sclerite aggregates) are arrowed at the tip and around polyp cavities. (c) Schematic representation of the C. rubrum anatomy. Internal polyp structure after Bayer (1956). The inset shows a SEM secondary electron image of a sclerite. Abbreviations: P: polyp; Cr: longitudinal crenulation.

Figure 2: Two-dimensional tomographic slices of a C. rubrum branch tip. (a) XZ tomographic slice of a µ-CT at 2 µm resolution of a branch tip showing the mineralized organic layer around the skeleton axis. Zones of contact between MOL and hard skeleton are circled. (b and c) XY slices of the same µ-CT at 2 µm resolution showing the MOL structure (superficial gastrodermal canal network arrowed in Fig. 2b). Direct contact between the MOL and the skeleton occurs only between two polyps (zones of contact arrowed in Fig. 2c). Abbreviations: P: polyp; MOL: mineralized organic layer; Sk: skeleton; Scl: sclerite.

Figure 3: Aggregated sclerites at a C. rubrum branch tip (a) SEM secondary electron image of cemented sclerites. (b) Enlargement of (a).

Figure 4: C. rubrum central core and annular domain. (a) SEM-BSE images of the central core of a perpendicular section. The central core is characterized by the presence of sclerites (small darker units with closed shape). The annular part is composed of contrasted layers corresponding to annual growth rings. (b) Magnification of (a) showing sclerites embedded

733 *within calcitic layers. The white line underlines the boundary between the central core and the*
734 *annular domain. (c) Electron microprobe (EMP) chemical map of magnesium in the same section*
735 *than (a). The brightest zones in the central core correspond to sclerites. The chemical*
736 *oscillations surrounding the central core correspond to annual growth rings. (d) EMP map of*
737 *sulfur showing that the central core is in average poorer in S than the annular part.*
738 *Abbreviations: An: annular domain; Co: central core; Sc: sclerites.*
739
740 *Figure 5: Longitudinal section of C. rubrum skeleton and sclerite aggregates. (a) Mosaic of*
741 *SEM-BSE images of a longitudinal section showing the core (circled in green) and annular*
742 *domains (circled in blue) and the mineralized organic layer (circled in yellow). (b) Enlargement*
743 *of the central core. Sclerites and sclerite aggregates are embedded within a calcitic cement with*
744 *high frequency contrast oscillations. (c) SEM image of a sclerite aggregate extracted from the*
745 *apical tissues. Abbreviations: MOL: mineralized organic layer; P: polyp; An: annular domain;*
746 *Co: central core; µ-prot: microprotuberance; Sc.Ag.: sclerite aggregate; Sc: sclerite.*
747
748 *Figure 6: C. rubrum annular domain. (a) EMP map of magnesium of a perpendicular section*
749 *showing the skeleton and the surrounding tissues. In order to enhance internal details in both the*
750 *tissues and the skeleton, the portions of image corresponding to each domain have been*
751 *processed separately. Thus, the uncalibrated grey scales are different in the two domains.*
752 *Skeleton and sclerite boundaries have been circled in white. Note the local discontinuities in the*
753 *skeleton layers (white arrows). (b) SEM-BSE image of a longitudinal section of skeleton with two*
754 *sclerites incorporated in the annular domain. Abbreviations: Sk: skeleton; MOL: mineralized*
755 *organic layer; Sc: sclerite; µ-prot: microprotuberance.*
756

Figure 7: EMP Chemical maps of magnesium and sulfur of a perpendicular section of C. elatius. (a) Low resolution magnesium map showing a three-pointed star shape corresponding to the central core with higher magnesium content. The surrounding annular part is characterized by oscillations of magnesium content. (b) High resolution magnesium map of the central core with characteristic more magnesian sclerites. (c) Sulfur map on the same area than (b); sclerites are characterized by low S contents. Abbreviations: An: annular domain; Co: central core; Sc: sclerite.

Figure 8: Structure of C. elatius (a) SEM-BSE image of a perpendicular section of C. elatius (same area and orientation as in Figs. 7b and c). (b) Enlargement of (a) displaying sclerites within the central core. (c) Another enlargement of the central core; the white line along the right hand side of the image indicates the boundary between the core and the annular domain. The sclerites are embedded within core calcitic layers with high frequency contrast oscillations. (d) SEM-BSE image of annual growth rings (white dashed lines) (see Fig. 7a for the location of the image). An isolated sclerite is observed in the annular layers (inset). Abbreviations: An: annular domain; Co: central core; Sc: sclerite.

Figure 9: Mg and S distribution in P. japonicum skeleton (a) Magnesium map of a perpendicular section of skeleton showing a portion of the core on the right hand side of the image. The growth rings are 150 µm wide in average. Crenulations are usually faint but locally well defined (white arrows). (b and c) Higher resolution Mg and S maps of the core of P. japonicum shown in (a). Abbreviations: An: annular domain; Co: core.

780 *Figure 10: Structure of P. japonicum skeleton. (a) SEM-BSE image of the core (same location*
781 *and orientation as in Fig. 9b). (b) Enlargement of a portion of (a) showing the sclerites within the*
782 *core and details of the inner structure of the sclerites. (c) SEM-BSE image of perpendicular*
783 *section (see location in Fig. 9a). Some growth rings are underlined in white. A sclerite embedded*
784 *within the annular layers is enlarged in the inset. Abbreviations as in Fig. 8.*
785
786 *Figure 11: Structure of C. johnsoni, C. niobe and P. thrinax. (a) SEM-BSE image of a*
787 *perpendicular section of C. johnsoni skeleton. (b) Enlargement of (a) with sclerites in the central*
788 *core. The white line marks the boundary between the core and the annular domain. (c) Mosaic of*
789 *SEM-BSE images of a perpendicular section of C. niobe skeleton. (d) Enlargement of (c) showing*
790 *the core and its sclerites. (e-f) Core-annular transition in P. thrinax at two different*
791 *magnifications. Abbreviations as in Fig.5.*
792
793 *Figure 12: A model for the skeleton growth of C. rubrum and other Corallium species. (a)*
794 *Longitudinal section of skeleton (red) surrounded by organic tissues composed of polyps (grey),*
795 *mineralized organic layer (orange) containing the sclerites (orange dots). Deep gastrodermal*
796 *canals (dark green) are located against the sub-apical skeleton while the superficial*
797 *gastrodermal canals (light green) are present everywhere within the mineralized organic layer.*
798 *Mesoglea devoid of sclerites is shown in yellow. At the tip, the sclerites are confined between the*
799 *polyps, and MOL and skeleton are in direct contact. In the sub-apical part, MOL and skeleton*
800 *are separated from each other by the deep gastrodermal canal network. The mineralizing*
801 *epithelium indicated in blue is discontinuous at the tip and continuous around the sub-apical*
802 *skeleton. The central core mainly constituted of sclerites cemented together is represented as*
803 *chaotic and discontinuous orange lines. The annular layers surrounding the core are represented*

804 *as more continuous red lines. (b), (c), (d) Radial sections at different growth stages. Scale bars*
805 *are indicative only, and the different organs of the organism are not perfectly at scale.*
806 *Abbreviations: P: polyp; Me: mesoglea without sclerites; MOL: mineralized organic layer; Epth:*
807 *mineralizing epithelium; Sc: sclerites; Co: central core; An: Annular domain; Dgc: deep*
808 *gastrodermal canal; Sgc: superficial gastrodermal canal.*
809
810

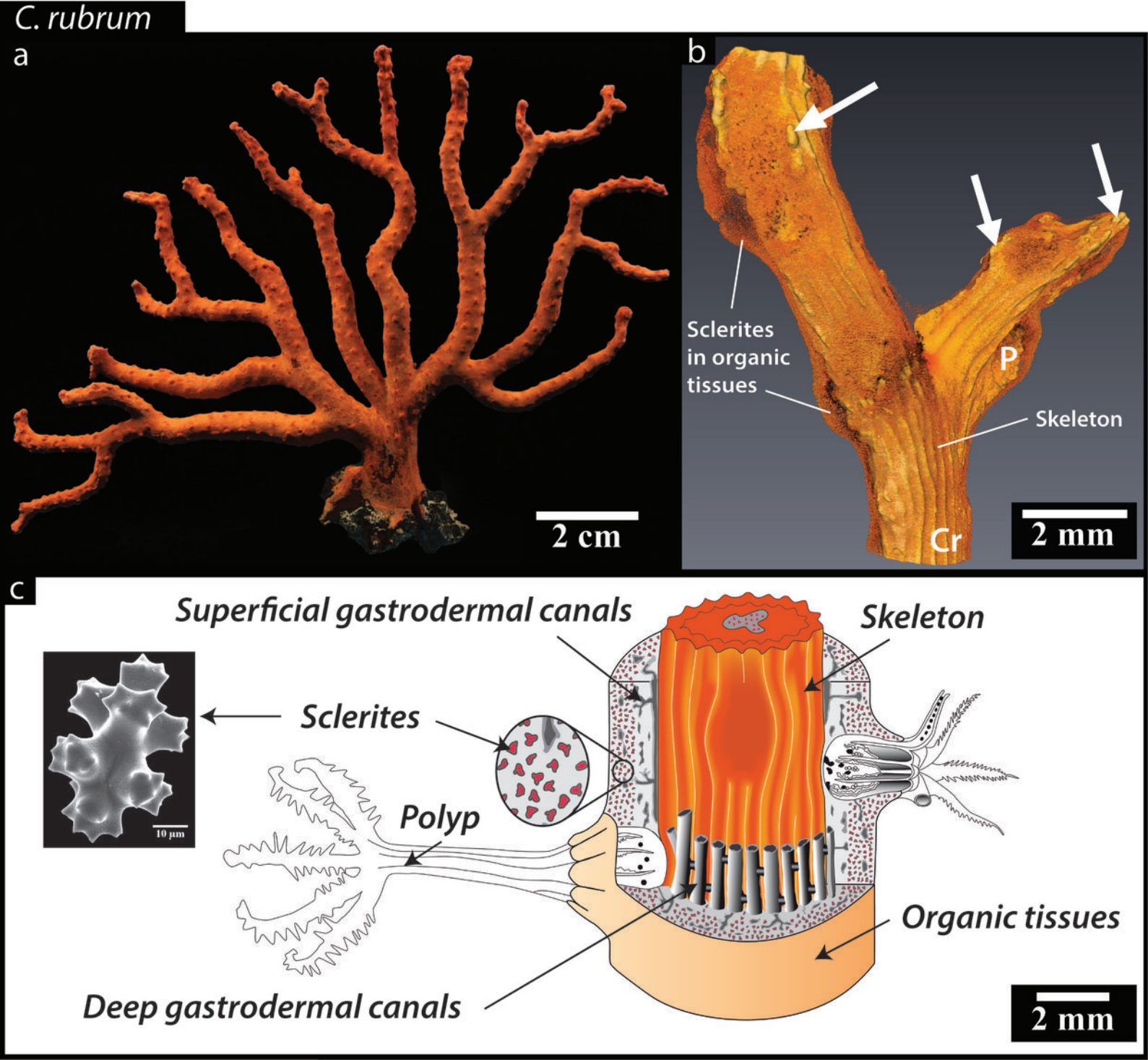
C. rubrum
a
2 cm
b
Sclerites
in organic
tissues
P
Skeleton
Cr
2 mm
c
Superficial gastrodermal canals
Skeleton
Sclerites
10 µm
Polyp
Organic tissues
Deep gastrodermal canals
2 mm

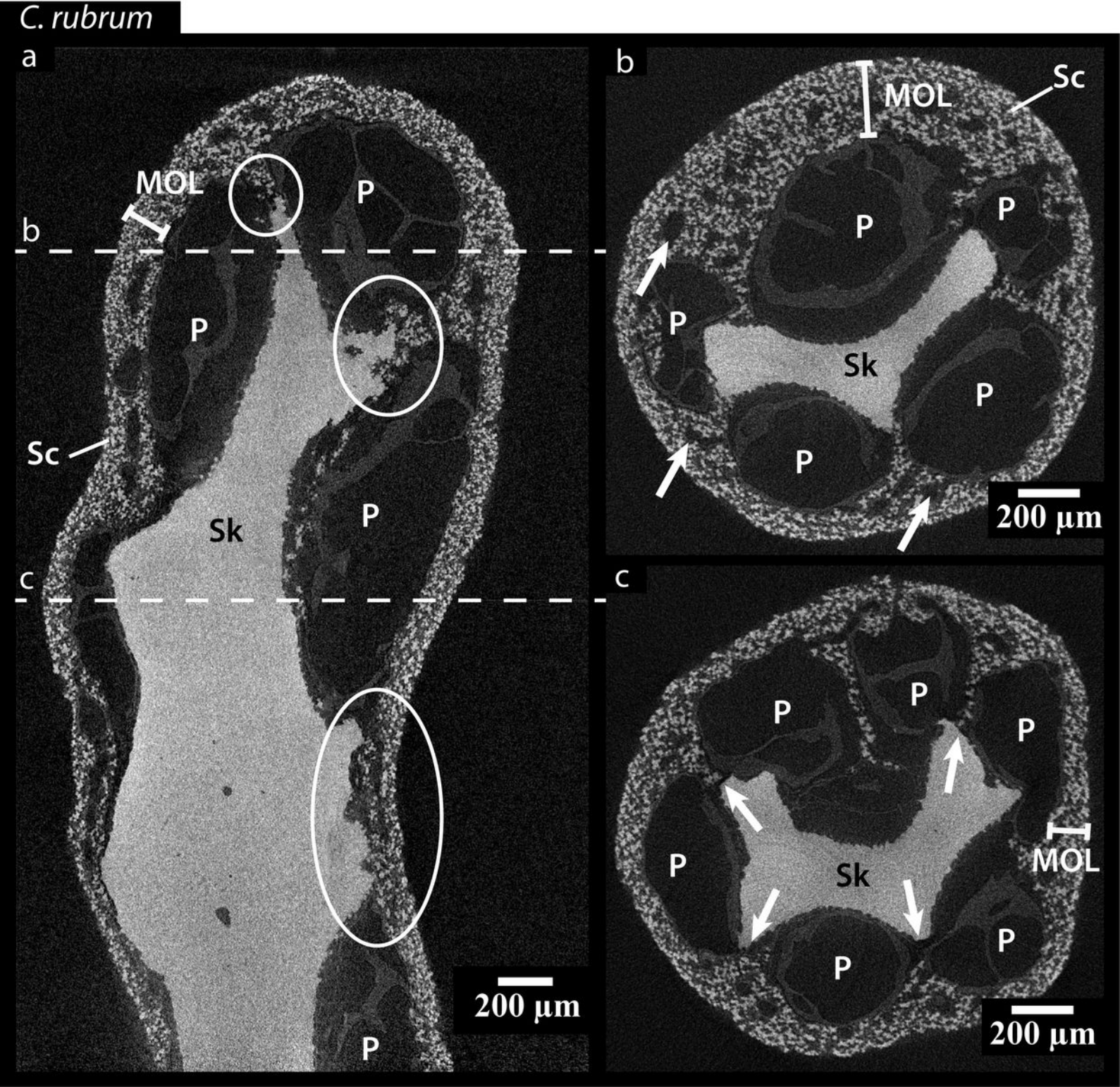
C. rubrum
a
MOL
P
b
P
Sc
Sk
P
c
200 µm
P
b
MOL
Sc
P
P
P
Sk
P
P
200 µm
c
P
P
P
P
Sk
MOL
P
P
P
200 µm

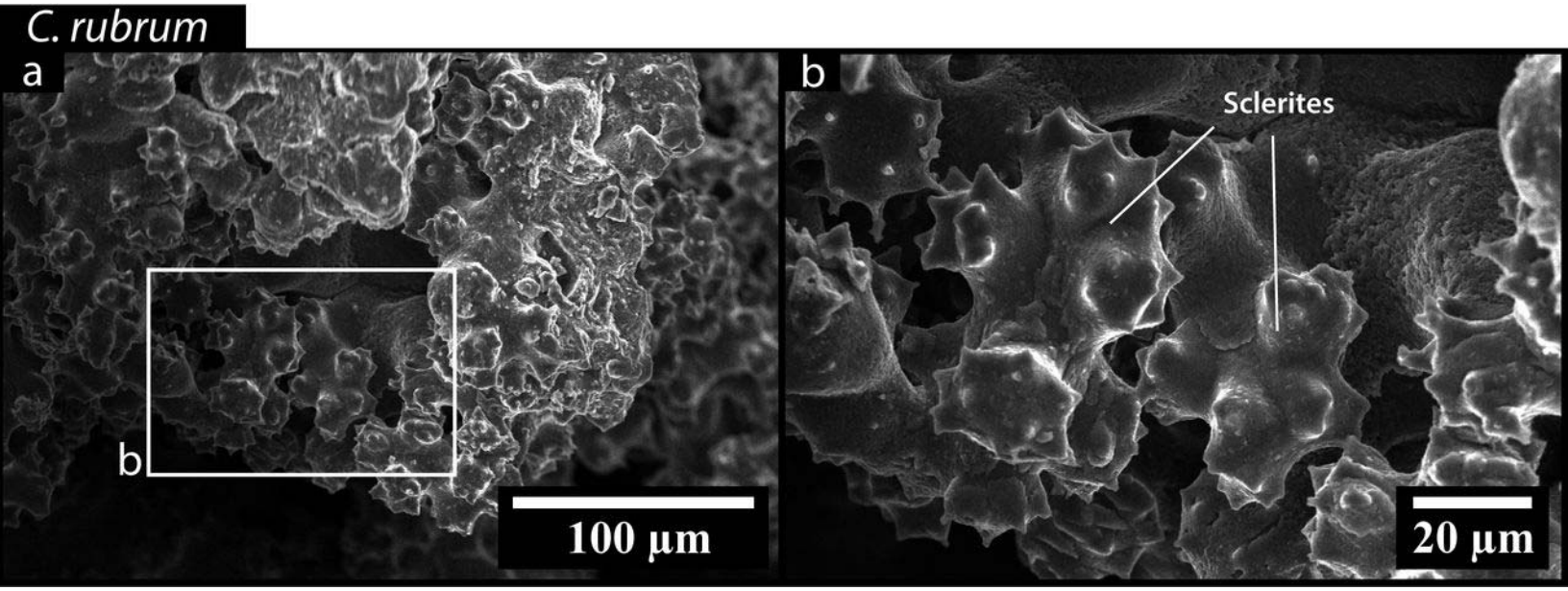
C. rubrum
a
b
100 µm
b
Sclerites
20 µm

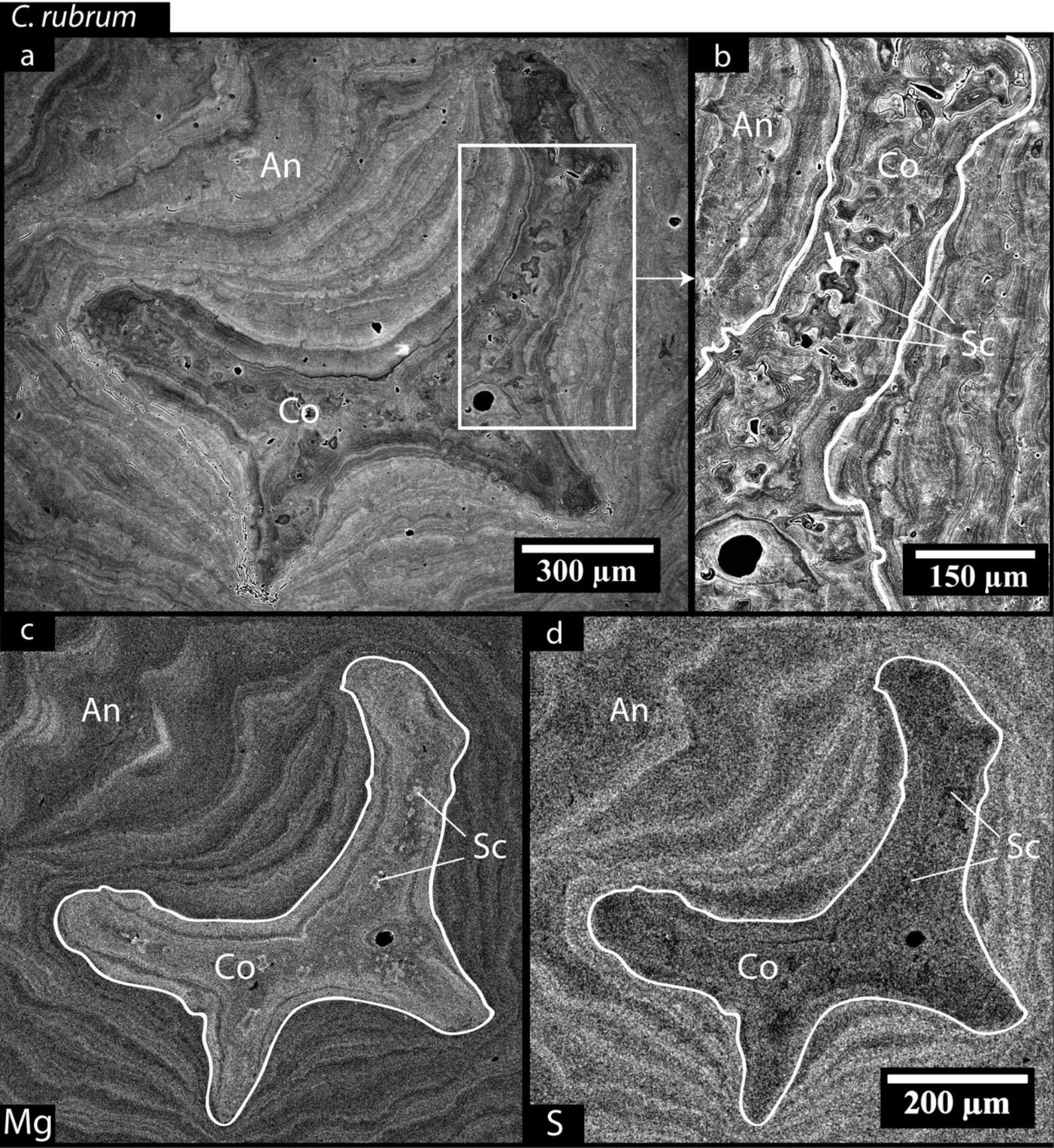
C. rubrum
a
An
Co
300 µm
b
An
Co
Sc
150 µm
c
An
Sc
Co
Mg
d
An
Sc
Co
S
200 µm

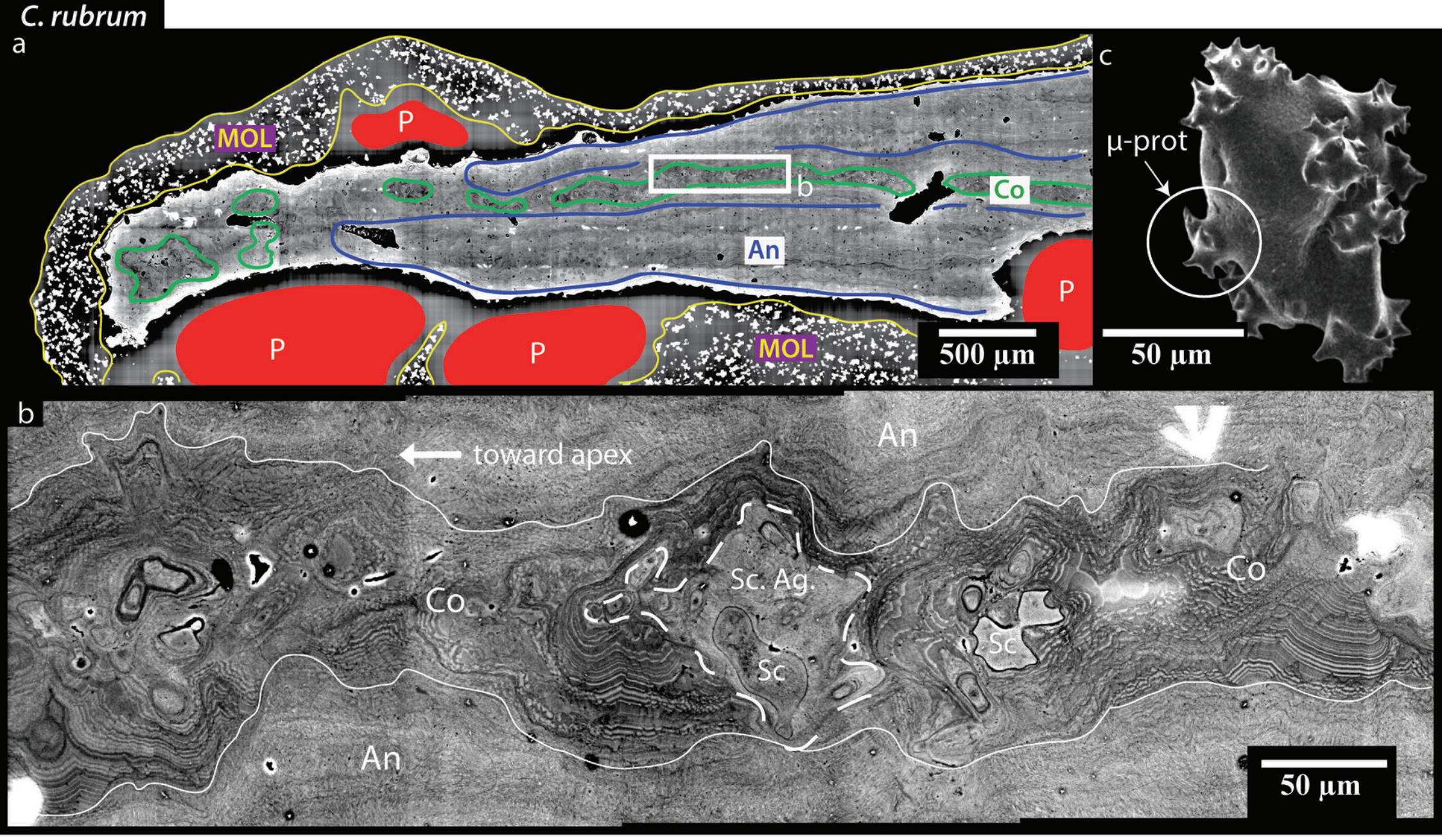
C. rubrum
a
MOL
P
b
Co
An
P
P
P
MOL
500 µm
c
µ-prot
50 µm
b
toward apex
An
Co
Sc. Ag.
Sc
Sc
Co
An
50 µm

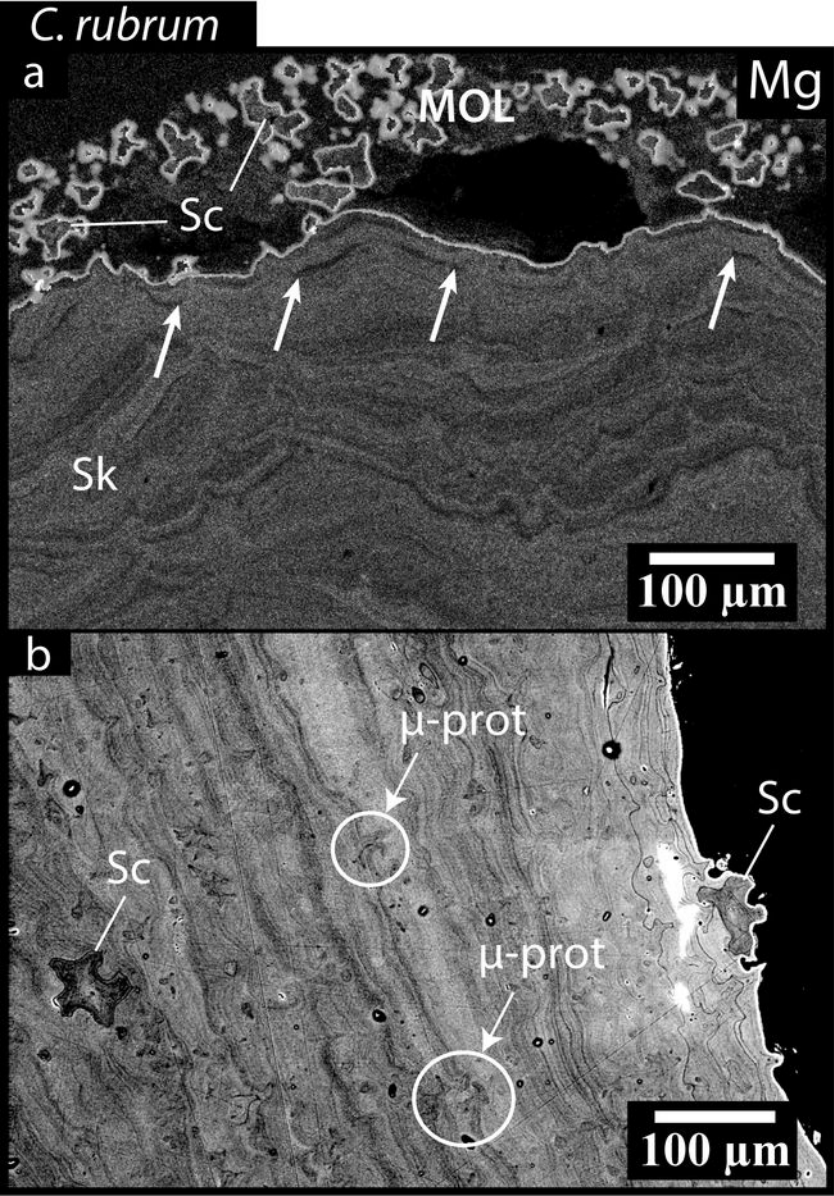
C. rubrum
a
Mg
MOL
Sc
Sk
100 µm
b
µ-prot
Sc
Sc
µ-prot
100 µm

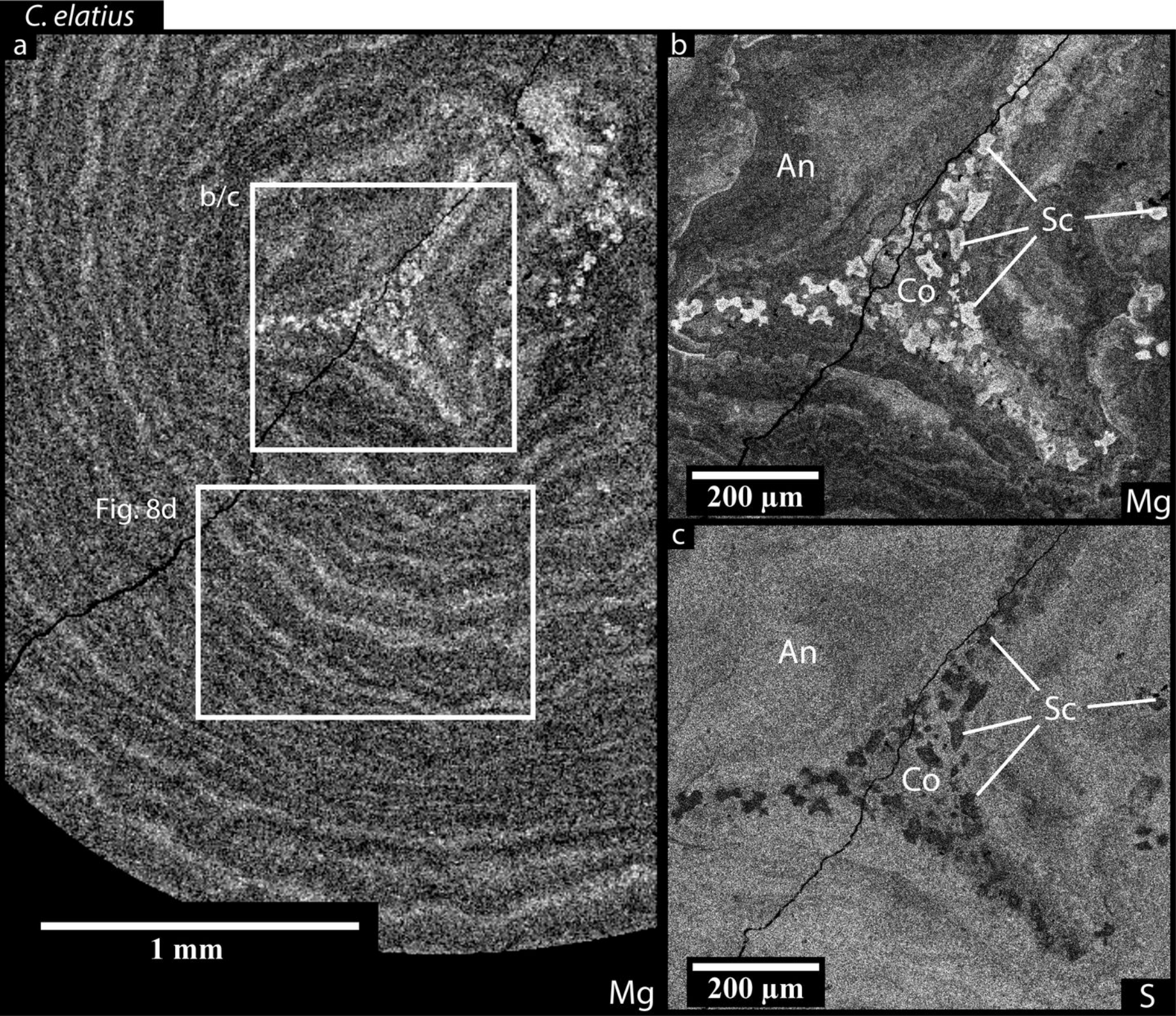
C. elatius
a
b/c
Fig. 8d
1 mm
Mg
b
An
Sc
Co
200 µm
Mg
c
An
Sc
Co
200 µm
S

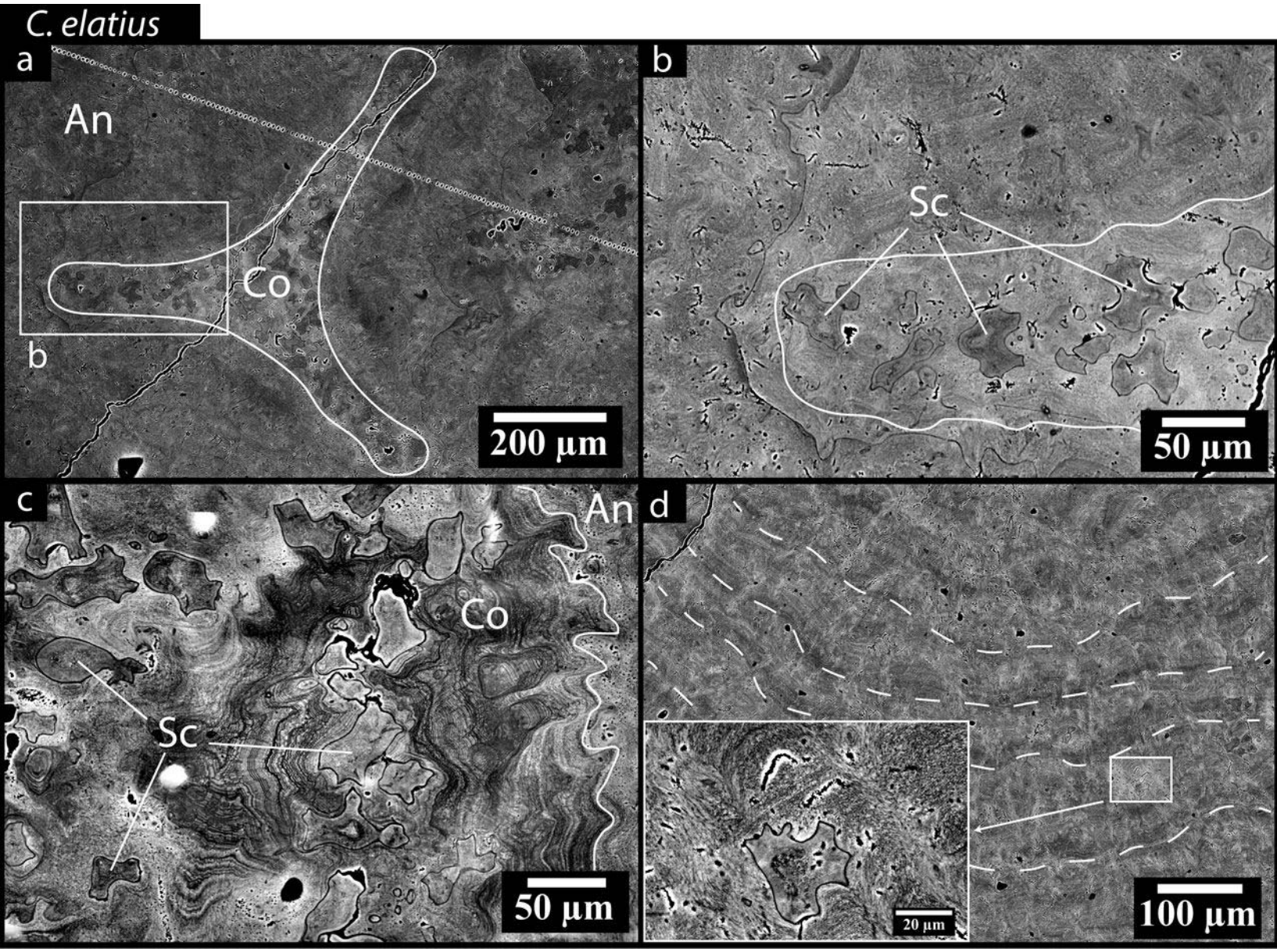
C. elatius
a
An
Co
b
200 µm
b
Sc
50 µm
c
An
Co
Sc
50 µm
d
20 µm
100 µm

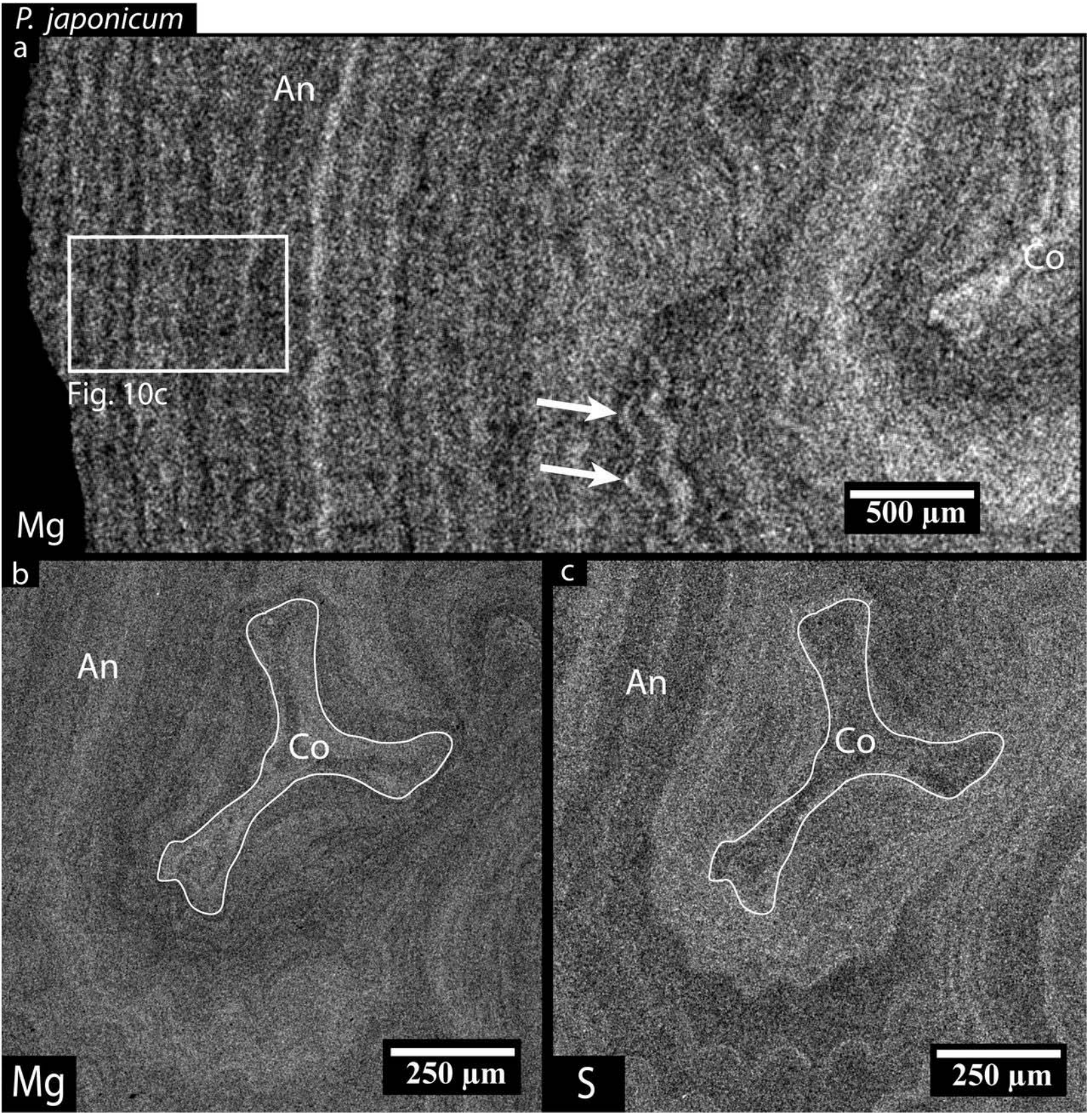
P. japonicum
a
An
Co
Fig. 10c
Mg
500 µm
b
An
Co
Mg
250 µm
c
An
Co
S
250 µm

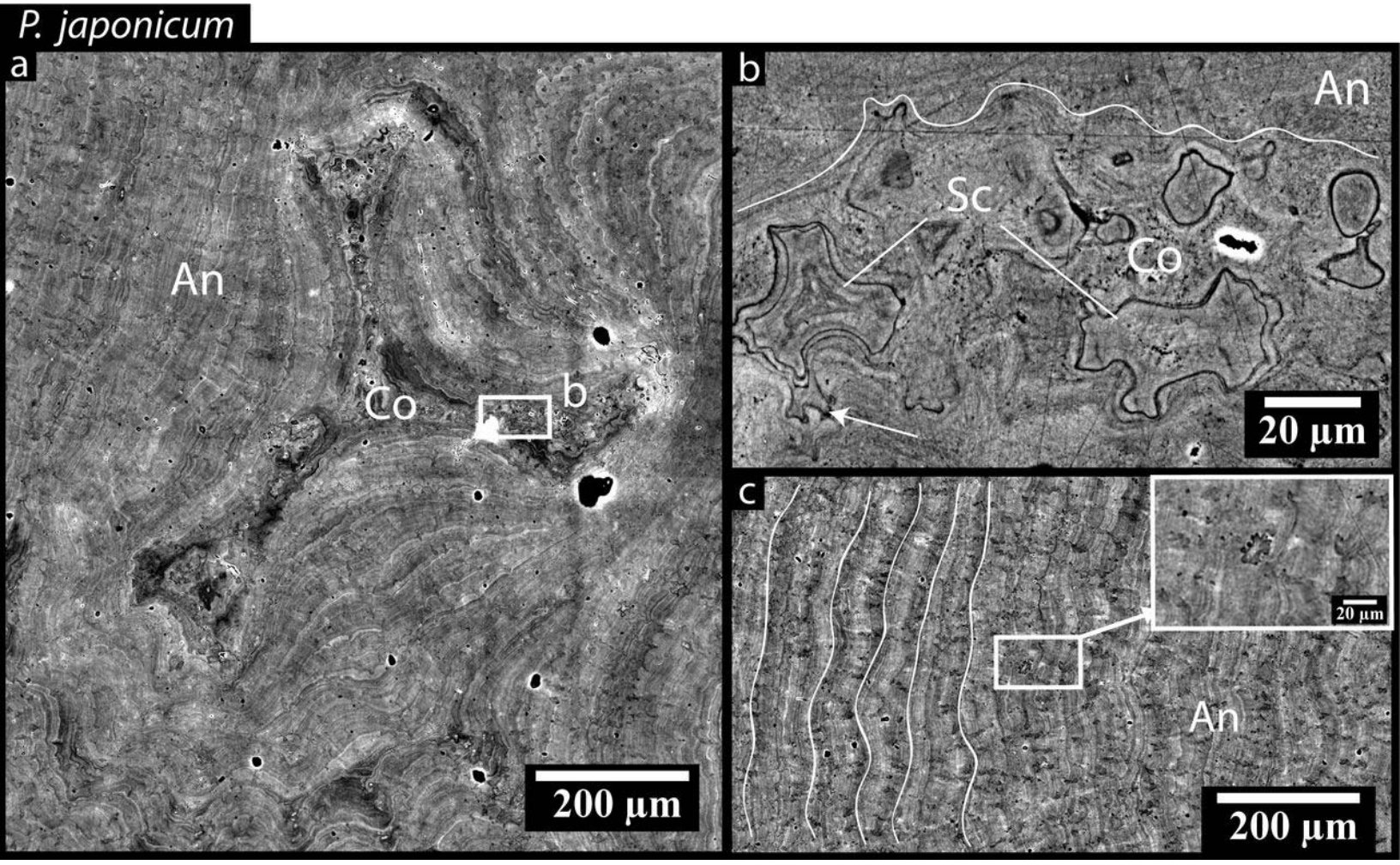
P. japonicum
a
An
Co
b
200 µm
b
An
Sc
Co
20 µm
c
20 µm
An
200 µm

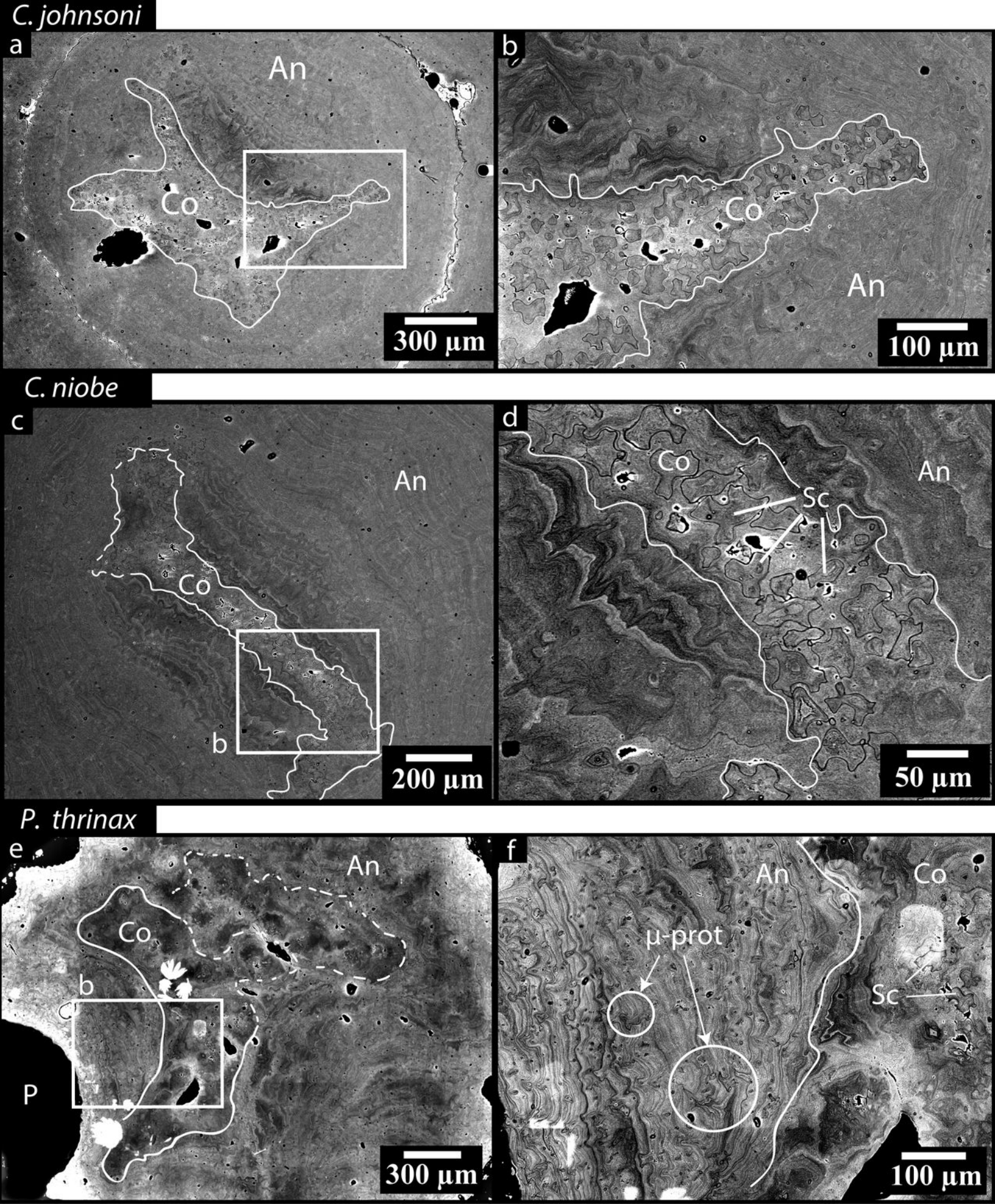
C. johnsoni
a
An
Co
300 µm
b
Co
An
100 µm
C. niobe
c
An
Co
b
200 µm
d
Co
Sc
An
50 µm
P. thrinax
e
An
Co
b
P
300 µm
f
An
Co
µ-prot
Sc
100 µm

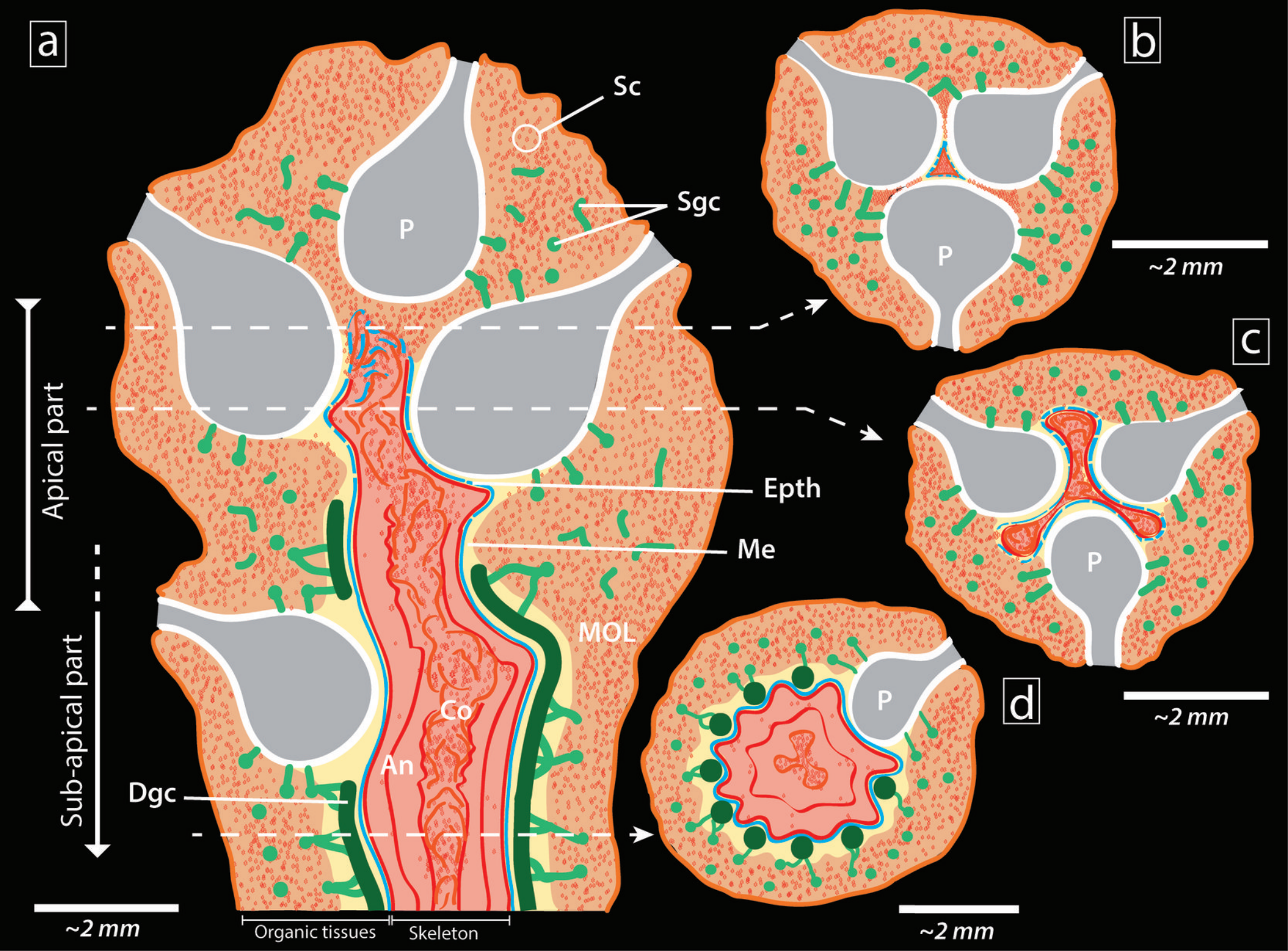
a
b
c
d
Sc
Sgc
P
Apical part
Sub-apical part
Epth
Me
MOL
Co
An
Dgc
Organic tissues
Skeleton
~2 mm
~2 mm
~2 mm
~2 mm